interfacing with the electrodes was not counted for all of these devices.
28. M. S. Dresselhaus, G. Dresselhaus, A. Jorio, A. G. Souza Filho, R. Saito, *Carbon* **40**, 2043 (2002).
29. A. Jorio *et al.*, *Phys. Rev. Lett.* **86**, 1118 (2001).
30. B. Zhao *et al.*, *J. Nanosci. Nanotechnol.* **4**, 995 (2004).
31. S. M. Keogh *et al.*, *J. Phys. Chem. B* **108**, 6233 (2004).
32. This research was partially supported by the NSF-sponsored Center for Polymer Interface and Macromolecular Assemblies (CPIMA), Samsung Advanced Research Institute of Technology, Intel, and Applied Materials. M.C.L. acknowledges support from the Intelligence Community Postdoctoral Fellowship Program. M.R. acknowledges support from the NASA Graduate Student Research Fellowship. Z.B. acknowledges support from the Sloan Research Fellowship and Finmeccanica Faculty Scholar Award. We thank S. Hellstrom, H. W. Lee, J. N. Kurtin (Intel), and B. Chen (NASA Ames) for technical discussions.

Supporting Online Material
www.sciencemag.org/cgi/content/full/321/5885/101/DC1
Materials and Methods
Figs. S1 to S11
Table S1
References

18 February 2008; accepted 29 May 2008
10.1126/science.1156588

Relativistic Spin Precession in the Double Pulsar

Rene P. Breton,[1]* Victoria M. Kaspi,[1] Michael Kramer,[2] Maura A. McLaughlin,[3,4] Maxim Lyutikov,[5] Scott M. Ransom,[6] Ingrid H. Stairs,[7] Robert D. Ferdman,[7,8] Fernando Camilo,[9] Andrea Possenti[10]

The double pulsar PSR J0737–3039A/B consists of two neutron stars in a highly relativistic orbit that displays a roughly 30-second eclipse when pulsar A passes behind pulsar B. Describing this eclipse of pulsar A as due to absorption occurring in the magnetosphere of pulsar B, we successfully used a simple geometric model to characterize the observed changing eclipse morphology and to measure the relativistic precession of pulsar B's spin axis around the total orbital angular momentum. This provides a test of general relativity and alternative theories of gravity in the strong-field regime. Our measured relativistic spin precession rate of $4.77^{\circ}{}^{+0^{\circ}.66}_{-0^{\circ}.65}$ per year (68% confidence level) is consistent with that predicted by general relativity within an uncertainty of 13%.

Spin is a fundamental property of most astrophysical bodies, making the study of its gravitational interaction an important challenge (*1*). Spin interaction manifests itself in different forms. For instance, we expect the spin of a compact rotating body in a binary system with another compact companion to couple gravitationally with the orbital angular momentum (relativistic spin-orbit coupling) and also with the spin of this companion (relativistic spin-spin coupling) (*2*, *3*). Observing such phenomena provides important tests for theories of gravity, because every successful theory must be able to describe the couplings and to predict their observational consequences. In a binary system consisting of compact objects such as neutron stars, one can generally consider the spin-orbit contribution acting on each body to dominate greatly the spin-spin contribution. This interaction results in a precession of the bodies' spin axis around the orbital angular momentum of the system, behavior we refer to as relativistic spin precession.

Although relativistic spin precession is well studied theoretically in general relativity (GR), the same is not true of alternative theories of gravity, and hence quantitative predictions of deviations from GR spin precession do not yet exist (*4*). For instance, it is expected that in alternative theories relativistic spin precession may depend on strong self-gravitational effects; that is, the actual precession may depend on the structure of a gravitating body (*4*). In the weak gravitational fields encountered in the solar system, these strong-field effects generally cannot be detected (*5*–*7*). Measurements in the strong-field regime near massive and compact bodies such as neutron stars and black holes are required. Relativistic spin precession has been observed in some binary pulsars [e.g., (*8*–*10*)], but it has usually only provided a qualitative confirmation of the effect. Recently, the binary pulsar PSR B1534+12 allowed the first quantitative measurement of this effect in a strong field, and although the spin precession rate was measured to low precision, it was consistent with the predictions of GR (*11*).

Here, we report a precision measurement of relativistic spin precession using eclipses observed in the double pulsar (*12*, *13*). This measurement, combined with observational access to both pulsar orbits in this system, allows us to constrain quantitatively relativistic spin precession in the strong-field regime within a general class of gravitational theories that includes GR.

PSR J0737–3039A/B consists of two neutron stars, both visible as radio pulsars, in a relativistic 2.45-hour orbit (*12*, *13*). High-precision timing of the pulsars, having spin periods of 23 ms and 2.8 s (hereafter called pulsars A and B, respectively), has already proven to be the most stringent test bed for GR in the strong-field regime (*14*) and enables four independent timing tests of gravity, more than any other binary system.

The orbital inclination of the double pulsar system is such that we observe the system almost perfectly edge-on. This coincidence causes pulsar A to be eclipsed by pulsar B at pulsar A's superior conjunction (*13*). The modestly frequency-dependent eclipse duration, about 30 s, corresponds to a region extending ~1.5×10^7 m (*15*). The light curve of pulsar A during its eclipse shows flux modulations that are spaced by half or integer numbers of pulsar B's rotational period (*16*). This indicates that the material responsible for the eclipse corotates with pulsar B. The relative orbital motions of the two pulsars and the rotation of pulsar B thus allow a probe of different regions of pulsar B's magnetosphere in a plane containing the line of sight and the orbital motion.

Synchrotron resonance with relativistic electrons is the most likely mechanism for efficient absorption of radio emission over a wide range of frequencies. In the model proposed by Lyutikov and Thompson (*17*), this absorbing plasma corotates with pulsar B and is confined within the closed field lines of a magnetic dipole truncated by the relativistic wind of pulsar A. The dipole magnetic moment vector makes an angle α with respect to the spin axis of pulsar B, whose orientation in space can be described by two angles: the colatitude of the spin axis with respect to the total angular momentum of the system, θ, and the longitude of the spin axis, ϕ (see Fig. 1 for an illustration of the system geometry). Additional parameters characterizing the plasma opacity, μ; the truncation radius of the magnetosphere, R_{mag}; and the relative position of pulsar A with respect to the projected magnetosphere of pulsar B, z_0, are also included in the model (*17*).

We monitored the double pulsar from December 2003 to November 2007 with the Green Bank Telescope in West Virginia; most of the data were acquired as part of the timing ob-

[1]Department of Physics, McGill University, Montreal, QC H3A 2T8, Canada. [2]Jodrell Bank Observatory, University of Manchester, Manchester M13 9PL, UK. [3]Department of Physics, West Virginia University, Morgantown, WV 26506, USA. [4]National Radio Astronomy Observatory, Green Bank, WV 24944, USA. [5]Department of Physics, Purdue University, West Lafayette, IN 47907, USA [6]National Radio Astronomy Observatory, Charlottesville, VA 22903, USA. [7]Department of Physics and Astronomy, University of British Columbia, Vancouver, BC V6T 1Z1, Canada. [8]Laboratoire de Physique et Chimie de l'Environnement–CNRS, F-45071 Orleans cedex 2, France. [9]Columbia Astrophysics Laboratory, Columbia University, New York, NY 10027, USA. [10]Osservatorio Astronomico di Cagliari, Istituto Nazionale di Astrofisica, Poggio dei Pini, 09012 Capoterra, Italy.

*To whom correspondence should be addressed. E-mail: bretonr@physics.mcgill.ca

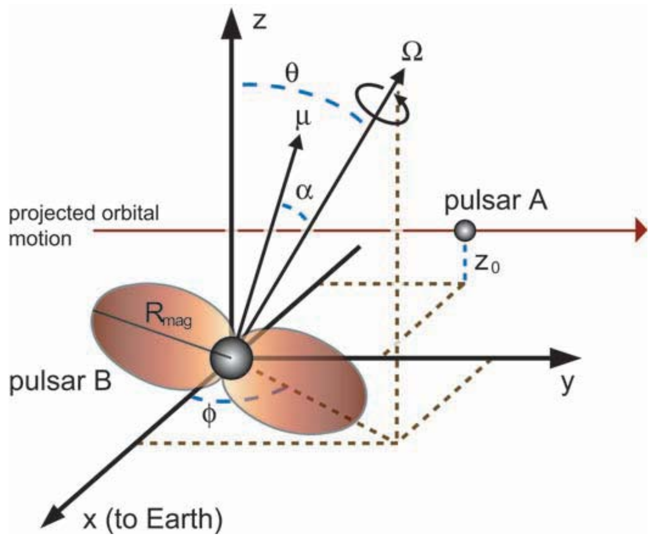

Fig. 1. Schematic view of the double pulsar system showing the important parameters for the modeling of pulsar A's eclipse (dimensions and angles are not to scale). Pulsar B is located at the origin of the cartesian coordinate system, whereas the projected orbital motion of pulsar A during its eclipse is parallel to the *y* axis at a constant z_0 as seen from Earth, which is located toward the positive *x* axis. Because the orbital inclination is almost perfectly edge-on (*14*), we can approximate the *z* axis to be coincident with the orbital angular momentum. The spin axis of pulsar B, whose spatial orientation is described by θ and ϕ, is represented by the Ω vector. The magnetic axis of pulsar B corresponds to the μ vector and makes an angle α with respect to Ω. Lastly, the absorbing region of the dipolar magnetosphere of pulsar B, truncated at radius R_{mag}, is shown as a shaded red region.

Fig. 2. Evolution of pulsar B's geometry as a function of time. The marginalized posterior probability distribution of the magnetic inclination (α), the colatitude of the spin axis (θ), and the longitude of the spin axis (ϕ) of pulsar B are shown from top to bottom, respectively. For each data point, the circle represents the median value of the posterior probability density, whereas the box and the bar indicate the 1σ and 3σ confidence intervals, respectively. The gray regions are the 3σ confidence regions derived from the joint time-dependent model fitting. For clarity, multiple eclipses are displayed as single data points when observed over an interval of about a week.

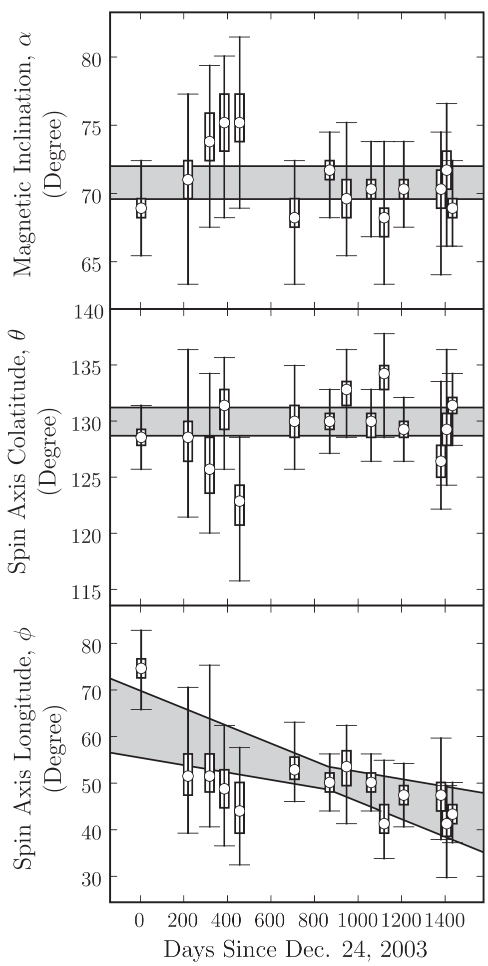

servations reported in (*14*). The data used for our analysis were taken at 820 MHz with the SPIGOT instrument (*18*), which provides 1024 frequency channels across a 50-MHz bandwidth. Data for a total of 63 eclipses of pulsar A were collected over the 4-year period, with many obtained during semi-annual concentrated observing campaigns. We dedispersed each eclipse data set by adding time shifts to frequency channels in order to compensate for the frequency-dependent travel time of radio waves in the ionized interstellar medium, and we then folded them at the predicted spin period of pulsar A by using the pulsar analysis packages PRESTO (*19*) and SIGPROC (*20*) [see (*14*) for details about the radio timing]. Next, we extracted the relative pulsed flux density of pulsar A by fitting each folded interval for the amplitude of a high signal-to-noise ratio pulse profile template made from the integrated pulse observed during the several-hour observation that includes each eclipse. Lastly, we normalized the flux densities so the average level outside the eclipse region corresponded to unity. We chose the time resolution of our eclipse light curves to equal, on average, four individual pulses of pulsar A (~91 ms).

In addition to the flux density, we determined the orbital phase and the spin phase of pulsar B corresponding to each data point of our time series. Orbital phases were derived from the ephemeris published in (*14*). Spin phases were empirically measured from data folded at the predicted period of pulsar B in a way similar to that described above for pulsar A. Over the 4-year monitoring campaign, we found notable changes in pulsar B's pulse profile, likely due to the precession of its spin axis, which were also reported in (*21*). Around 2003, the average pulse profile was unimodal, resembling a Gaussian function. It evolved such that, by 2007, it displayed two narrow peaks. Using the pulse peak maximum as a fiducial reference point is certainly not appropriate. We find, however, that the unimodal profile gradually became wider and then started to form a gap near the center of its peak. Since then, the outer edges of the pulse profile have not significantly changed, but the gap evolved such that two peaks are now visible. This lets us presume that the underlying average profile is reminiscent of a Gaussian-like profile to which some "absorption" feature has been superimposed near the center, leaving a narrow peak on each side. We therefore defined the fiducial reference point to lie at the center of the unimodal "envelope" that we reconstructed from the first 10 Fourier bins of the pulse profile, which contains 512 bins in total (see fig. S2 for an illustration of the pulse profile evolution).

We implemented the eclipse modeling of our data in two steps: the fitting of individual eclipse profiles and the search for evolution of the geometry of pulsar B. We first searched the full phase space to identify best-fit values of six parameters [see supporting online material (SOM) for more details]. Then, we reduced the number of free parameters to the subset (θ, ϕ, and α) describing the orientation of pulsar B's spin and magnetic axes by fixing the other parameters to their best-fit values: $\mu = 2$, $R_{mag} = 1.29°$ (projected value in terms of orbital phase), and $z_0/R_{mag} = -0.543$ (Fig. 1). Lastly, we performed a high-resolution mapping of the likelihood of this subspace in order to investigate subtle changes in the geometry. Lyutikov and Thompson (*17*) predicted that such changes, because of relativistic spin precession, could affect the eclipse light curve. In principle, relativistic spin precession of pulsar B's spin axis around the total angular momentum should induce a secular change of the longitude of the spin axis, ϕ, whereas the magnetic inclination, α, and the colatitude of the spin axis, θ, are expected to remain fixed over time. Indeed, from model fitting, we find no significant time evolution of α and θ, whereas ϕ does change. Because of correlation between the parameters, we jointly evaluated the best-fit geometry of pulsar B by using a time-dependent model in which $\alpha = \alpha_0$ and $\theta = \theta_0$ are constants and ϕ varies linearly with time; i.e., $\phi = \phi_0 - \Omega_B t$, where Ω_B is the rate of change of pulsar B's spin axis longitude and the epoch of $\phi = \phi_0$ is 2 May 2006 [Mean Julian Day (MJD) 53857]. Figure 2 shows the time evolution of the parameters and the fit derived from this joint time-dependent model (Table 1). The precession rate Ω_B of $4.77°^{+0°.66}_{-0°.65}$ year^{-1} (*22*) agrees with the precession rate predicted by GR (*23*), 5.0734° ± 0.0007° year^{-1} (*24*), within an uncertainty of 13% (68% confidence level).

This relatively simple model (*17*) is able to reproduce the complex phenomenology of the eclipses (Fig. 3 and movie S1) except at the eclipse boundaries, where slight magnetospheric distortions or variations in plasma density are likely to occur. Fits including the egress generally are poor in the central region where we observe narrow modulation features, which are critical for determining pulsar B's geometry. For this reason, we excluded the egress from the fits, using orbital phases between −1.0° and 0.75° (Fig. 3). We accounted for systematics introduced by the choice of the region to fit in the priors of our Bayesian model (SOM). This improved the fit of the model throughout the center region of the eclipse while still producing qualitatively good predictions near the eclipse egress. The overall success of the model implies that the geometry of pulsar B's magnetosphere is accurately described as predominantly dipolar; a pure quadrupole, for instance, does not reproduce the observed light curves. Although the model does not exclude the possibility that higher-order multipole components may exist close to the surface of pulsar B, our modeling supports the conclusions (*17*) that these eclipses yield direct empirical evidence supporting the long-standing assumption that pulsars have mainly dipolar magnetic fields far from their surface.

The direct outcome from modeling the eclipse profile evolution is a measurement of the effect of relativistic spin precession (see movie S2 for an illustration of the time evolution of the eclipse). We can use the inferred precession rate to test GR (Fig. 4) and to further constrain alternative theories of gravity and the strong-field aspects of relativistic spin precession. We use the generic class of relativistic theories that are fully conservative (Lorentz-invariant) and based on a Lagrangian, as introduced by Damour and Taylor (*4*). In this way, we can study the constraints of our observations on theories of gravity by describing the spin-orbit interaction within a specific theory that couples functions appearing in the corresponding part of the Lagrangian. In this framework, we can write the precession rate of pulsar B in a general form, $\Omega_B = \sigma_B L / a^3_R (1 - e^2)^{3/2}$, where L is the orbital angular momentum of the system, a_R is the semimajor axis of the relative orbit between the pulsars, e the eccentricity of the orbit, and σ_B is a generic strong-field spin-orbit coupling constant. Because L and a_R are not directly measurable, it is more convenient to write the above expression with use of observable Keplerian and post-Keplerian parameters. Although alternative forms generally involve a mixture of gravitational theory–dependent terms, the particular choice $\Omega_B = \frac{x_A x_B}{s^2} \times \frac{n^3}{1-e^2} \times \frac{c^2 \sigma_B}{G}$ is the only one that does not incorporate further theoretical terms other than the spin-orbit coupling constant, σ_B; the speed of light, c; and a generalized gravitational constant for the interaction between the two pulsars, G. In this expression, the Keplerian parameters e and $n = 2\pi/P_b$, the angular orbital frequency, are easily measurable for any binary system. On the other hand, the post-Keplerian Shapiro delay shape parameter, s, equivalent to the sine of the orbital inclination angle (*4*), requires relatively edge-on orbits to be observed. Measurement of the projected semi-major axes of the two orbits (*25*), x_A and x_B, found in the above equation necessitates that each body must be able to be timed. Therefore, the double pulsar is the only relativistic binary system that allows a direct constraint on the spin-orbit coupling in general theories of gravity. By using the inferred preces-

Table 1. Geometrical parameters of pulsar B derived from the eclipse model fitting. The presented values include priors related to systematic uncertainties. The epoch of $\phi = \phi_0$ is 2 May 2006 (MJD 53857).

Parameter	Mean	Median	68.2% confidence	99.7% confidence
α_0	70.92°	70.94°	(70.49°, 71.31°)	(69.68°, 72.13°)
θ_0	130.02°	130.02°	(129.58°, 130.44°)	(128.79°, 131.37°)
ϕ_0	51.21°	51.20°	(50.39°, 52.03°)	(48.80°, 53.72°)
Ω_B	4.77° year^{-1}	4.76° year^{-1}	(4.12°, 5.43°) year^{-1}	(2.89°, 6.90°) year^{-1}

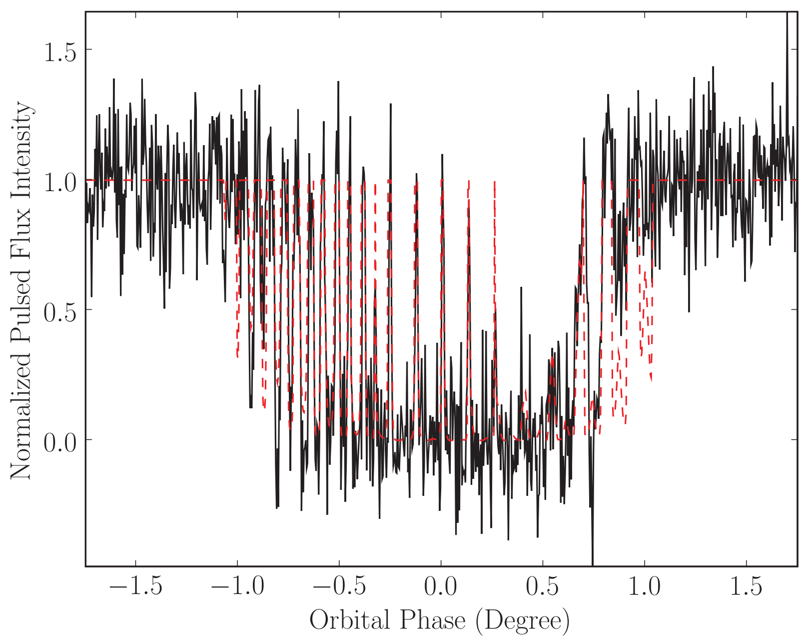

Fig. 3. Average eclipse profile of pulsar A consisting of eight eclipses observed at 820 MHz over a 5-day period around 11 April 2007 (black line) along with a model eclipse profile (red dashed line). The relative pulsed flux density of pulsar A is normalized so that the average level outside the eclipse region is unity. The resolution of each data point is ~91 ms, whereas 1° in orbital phase corresponds to 24.5 s. Near orbital phase 0.0, the spikes are separated by the spin period of pulsar B.

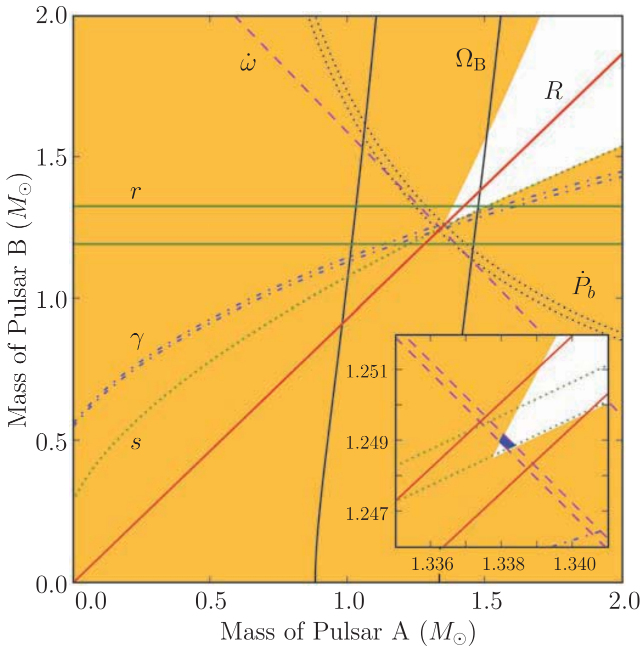

Fig. 4. Mass-mass diagram illustrating the present tests constraining general relativity in the double pulsar system. (**Inset**) An expanded view of the region where the lines intersect. If general relativity is the correct theory of gravity, all lines should intersect at common values of masses. The mass ratio ($R = x_B/x_A$) and five post-Keplerian parameters (s and r, Shapiro delay shape and range; $\dot{\omega}$, periastron advance; $\dot{P}_b$, orbital period decay due to the emission of gravitational waves; and γ, gravitational redshift and time dilation) were reported in (*14*). Shaded orange regions are unphysical solutions because $\sin i \leq 1$, where i is the orbital inclination. In addition to allowing a test of the strong-field parameter $\left(\frac{c^2\sigma_B}{G}\right)$, the spin precession rate of pulsar B, Ω_B, yields a new constraint on the mass-mass diagram. $M_\odot$ is the mass of the Sun.

sion rate of $\Omega_B = 4.77°^{+0°.66}_{-0°.65}$ year^{-1}, we derive $\left(\frac{c^2\sigma_B}{G}\right) = 3.38^{+0.49}_{-0.46}$. Every successful theory of gravity in the given generic framework must predict this value: These observations provide a strong-field test of gravity that complements and goes beyond the weak-field tests of relativistic spin precession (*26*). In GR, we expect to measure $\left(\frac{c^2\sigma_B}{G}\right)_{GR} = 2 + \frac{3}{2}\frac{m_A}{m_B} = 3.60677 \pm 0.00035$, where we have used the masses determined from the precisely observed orbital precession and the Shapiro delay shape parameter under the assumption that GR is correct (*14*). Comparing the observed value with GR's predictions, we find $\left(\frac{c^2\sigma_B}{G}\right)_{obs} / \left(\frac{c^2\sigma_B}{G}\right)_{GR} = 0.94 \pm 0.13$. Hence, GR passes this test of relativistic spin precession in a strong-field regime, confirming, within uncertainties, GR's effacement property of gravity even for spinning bodies, that is, the notion that strong internal gravitational fields do not prevent a compact rotating body from behaving just like a spinning test particle in an external weak field (*27*).

The spin precession rate, as well as the timing parameters entering in the calculation of $\left(\frac{c^2\sigma_B}{G}\right)$, are all independent of the assumed theory of gravity. If the main contribution limiting the precision of this new strong-field test comes from the inferred spin precession rate, we expect that the statistical uncertainty should decrease significantly with time, roughly as the square of the monitoring baseline for similar quantity and quality of eclipse data. The contribution of systematics to the error budget should also decrease, but its functional time dependence is difficult to estimate. Although the orbital and spin phases of pulsar B are input variables to the eclipse model, our ability to determine the orientation of pulsar B in space does not require the degree of high-precision timing needed for measurement of post-Keplerian parameters; evaluating spin phases to the percent level, for instance, is sufficient. Therefore, the intrinsic correctness of the model and its ability to reproduce future changes in the eclipse profile because of evolution of the geometry are the most likely limitations to improving the quality of this test of gravity, at least until the measured precession rate reaches a precision comparable with the timing parameters involved in the calculation of $\left(\frac{c^2\sigma_B}{G}\right)$. Better eclipse modeling could be achieved from more sensitive observations, and thus new-generation radio telescopes such as the proposed Square Kilometer Array could help make important progress. Pulsar A does not show evidence of precession (*28*, *29*) likely because its spin axis is aligned with the orbital angular momentum; it should therefore always remain visible, thus allowing long-term monitoring of its eclipses. Pulsar B, however, could disappear if spin precession causes its radio beam to miss our line of sight (*21*). In this event, we would need to find a way to circumvent the lack of observable spin phases for pulsar B, which are necessary to the eclipse fitting.

References and Notes

1. C. Will, *Living Rev. Relativity* **4**, 4 (2001).
2. The contribution from a classical quadrupolar moment is negligible for compact bodies.
3. R. F. O'Connell, in *Experimental Gravitation: Proceedings of Course 56 of the International School of Physics "Enrico Fermi,"* B. Bertotti, Ed. (Academic Press, New York, 1974), p. 496.
4. T. Damour, J. H. Taylor, *Phys. Rev. D* **45**, 1840 (1992).
5. T. Damour, G. Esposito-Farèse, *Phys. Rev. D* **46**, 4128 (1992).
6. T. Damour, G. Esposito-Farèse, *Class. Quantum Gravity* **9**, 2093 (1992).
7. T. Damour, G. Esposito-Farèse, *Phys. Rev. D* **53**, 5541 (1996).
8. J. M. Weisberg, R. W. Romani, J. H. Taylor, *Astrophys. J.* **347**, 1030 (1989).
9. M. Kramer, *Astrophys. J.* **509**, 856 (1998).
10. A. W. Hotan, M. Bailes, S. M. Ord, *Astrophys. J.* **624**, 906 (2005).
11. I. H. Stairs, S. E. Thorsett, Z. Arzoumanian, *Phys. Rev. Lett.* **93**, 141101 (2004).
12. M. Burgay *et al.*, *Nature* **426**, 531 (2003).
13. A. G. Lyne *et al.*, *Science* **303**, 1153 (2004); published online 8 January 2004 (10.1126/science.1094645).
14. M. Kramer *et al.*, *Science* **314**, 97 (2006); published online 14 September 2006 (10.1126/science.1132305).
15. V. M. Kaspi *et al.*, *Astrophys. J.* **613**, L137 (2004).
16. M. A. McLaughlin *et al.*, *Astrophys. J.* **616**, L131 (2004).
17. M. Lyutikov, C. Thompson, *Astrophys. J.* **634**, 1223 (2005).
18. D. L. Kaplan *et al.*, *Publ. Astron. Soc. Pacific* **117**, 643 (2005).
19. S. M. Ransom, S. S. Eikenberry, J. Middleditch, *Astrophys. J.* **124**, 1788 (2002). PRESTO is freely available at www.cv.nrao.edu/~sransom/presto/.
20. D. R. Lorimer. SIGPROC is freely available at http://sigproc.sourceforge.net.
21. M. Burgay *et al.*, *Astrophys. J.* **624**, L113 (2005).
22. Unless otherwise stated, uncertainties are quoted at the 68% confidence level.
23. B. M. Barker, R. F. O'Connell, *Phys. Rev. D* **12**, 329 (1975).
24. The uncertainty on the predicted GR spin precession rate arises because the value depends on the masses of the system, which are determined from two measured post-Keplerian parameters: the Shapiro delay s parameter and the advance of periastron, $\dot{\omega}$.
25. The projected semi-major axes are expressed in terms of light travel time across the orbit.
26. R. F. O'Connell, http://arxiv.org/abs/0804.3806 (2008).
27. T. Damour in *Three Hundred Years of Gravitation*, S. W. Hawking, W. Israel, Eds. (Cambridge Univ. Press, Cambridge, 1987), pp. 128–198.
28. R. N. Manchester *et al.*, *Astrophys. J.* **621**, L49 (2005).
29. R. D. Ferdman *et al.*, *40 Years of Pulsars: Millisecond Pulsars, Magnetars and More*, vol. 983 of *American Institute of Physics Conference Series*, C. Bassa, Z. Wang, A. Cumming, V. M. Kaspi, Eds. (American Institute of Physics, Melville, NY, 2008), pp. 474–478.

30. We thank N. Wex, T. Damour, R. F. O'Connell, R. D. Blandford, and W. G. Unruh for stimulating discussions. The National Radio Astronomy Observatory is a facility of the NSF operated under cooperative agreement by Associated Universities, Incorporated. This work was supported in part by the Natural Sciences and Engineering Research Council Discovery Grant program, the Canada Foundation for Innovation, the Canadian Institute for Advanced Research, an FQRNT (Le Fonds Québécois de la Recherche sur la Nature et les Technologies) team grant, the Canada Research Chair Program, the McGill University Lorne Trottier Chair in Astrophysics and Cosmology, and the Ministero dell'Istruzione dell'Università e della Ricerca under the grant PRIN-2005024090.

Supporting Online Material

www.sciencemag.org/cgi/content/full/321/5885/104/DC1
Materials and Methods
Figs. S1 and S2
References
Movies S1 and S2

18 April 2008; accepted 4 June 2008
10.1126/science.1159295